



Article

# Synthesis of Nitrogen-Doped Graphene on Copper Nanowires for Efficient Thermal Conductivity and Stability by Using Conventional Thermal Chemical Vapor Deposition

Minjeong Park <sup>1</sup> , Seoul-Ki Ahn <sup>1</sup>, Sookhyun Hwang <sup>1</sup>, Seongjun Park <sup>1</sup>, Seonpil Kim <sup>2</sup> and Minhyon Jeon <sup>1,\*</sup>

<sup>1</sup> Department of Nanoscience and Engineering, Center for Nano Manufacturing, Inje University, Gimhae 50834, Korea

<sup>2</sup> Department of Military Information Science, Gyeongju University, Gyeongju 38065, Korea

\* Correspondence: mjeon@inje.ac.kr; Tel.: +82-055-320-3672

Received: 11 June 2019; Accepted: 2 July 2019; Published: 7 July 2019



**Abstract:** Cu nanowires (NWs) possess remarkable potential as a low-cost heat transfer material in modern electronic devices. However, Cu NWs with high aspect ratios undergo surface oxidation, resulting in performance degradation. A growth temperature of approximately <math>1000\text{ }^\circ\text{C}</math> is required for preventing the changing of Cu NW morphology by the melting of Cu NWs at over <math>1000\text{ }^\circ\text{C}</math>. In addition, nitrogen (N)-doped carbon materials coated on Cu NWs need the formation hindrance of oxides and high thermal conductivity of Cu NWs. Therefore, we investigated the N-doped graphene-coated Cu NWs (NG/Cu NWs) to enhance both the thermal conductivity and oxidation stability of Cu NWs. The Cu NWs were synthesized through an aqueous method, and ethylenediamine with an amine group induced the isotropic growth of Cu to produce Cu NWs. At that time, the amine group could be used as a growth source for the N-doped graphene on Cu NWs. To grow an N-doped graphene without changing the morphology of Cu NWs, we report a double-zone growth process at a low growth temperature of approximately <math>600\text{ }^\circ\text{C}</math>. Thermal-interface material measurements were conducted on the NG/Cu NWs to confirm their applicability as heat transfer materials. Our results show that the synthesis technology of N-doped graphene on Cu NWs could promote future research and applications of thermal interface materials in air-stable flexible electronic devices.

**Keywords:** copper nanowires; N-doped graphene; chemical vapor deposition; growth; double-zone growth process; thermal interface materials

## 1. Introduction

The performance enhancement and long-term reliability of microelectronic devices are decidedly key issues in a wide range of electronic applications. Non-efficient heat dissipation in such devices leads to many problems, such as malfunction, decreased performance, and short-term stability as the power densities are increased. Therefore, effective heat transfer from integrated circuit to heat sink should contribute to the development of modern electronic devices [1–8].

Recently, various nanostructures, such as nanowires (NWs) [9–13] and nanoparticles [14–17], have been successfully synthesized as heat-transfer materials. Among these, NWs are more suitable as heat-transfer materials, owing to their natural continuity as well as high aspect ratio, which could lead to lower percolation thresholds. Their characteristics, such as wire diameter, density of wires in the network, and junction resistance substantially affect the physical properties [18,19]. Conventional metal NWs, especially Cu NWs, have a number of advantages, such as low cost, abundance on Earth, and has

a similar electrical conductivity to silver. Therefore, NWs possess remarkable potential as low-cost heat-transfer materials in modern electronic devices. However, Cu NWs with high aspect ratios could be intrinsically unstable under ambient conditions. The rapid surface oxidation of Cu NWs weakens their physical properties [20,21]. Several efforts have been made to prevent the surface oxidation of Cu NWs [22–30]. One approach is to provide a protection layer using graphene [28–30]. Carbon materials, such as carbon nanotubes and graphene, have been widely studied as heat-transfer materials based on their high intrinsic thermal conductivities, which range from 3000–6000 W/m·K [8]. Here, to realize effective heat transfer materials, various types of graphene are needed. The high thermal conductivity and formation hindrance of oxides on Cu NWs are also of great technological importance. Doping Cu NWs with other elements is a promising way to achieve this goal. Especially, nitrogen (N)-doped graphene promises many fascinating properties and widespread potential applications, such as super conduction [31], ferromagnetism [32], and has high thermal conductivity and the formation hindrance of oxides, such as CuO, Cu<sub>2</sub>O, and Cu(OH)<sub>2</sub>. Therefore, intensive theoretic studies are focused on N-doped graphene, and many theoretic models of the substitutionary-doped graphene have been established [33–37]. However, these studies are only based on theory, and an experimental example of the substitutionary N-doped graphene is still lacking, attributed to the limitations of synthetic methods. For decades, chemical vapor deposition (CVD) has been used as the general method for growing graphitic or doped graphitic [33–38] thin films. However, growing graphene directly onto Cu NWs is very difficult because a conventional thermal CVD (T-CVD) process requires a high process temperature of approximately 1000 °C.

In this study, we demonstrated N-doped graphene-coated Cu NWs (NG/Cu NWs) as the heat-transfer materials synthesized using a conventional T-CVD. To achieve a low temperature growth by using a conventional T-CVD, we used the double-zone growth process (DZGP) and succeeded in growing graphene on Cu NWs at a low temperature. Here, the Cu NWs with an amine group was used for the N-doped graphene. We realized the synthesis of the substitutionary NG/Cu NWs. Moreover, the experimental measurements of the morphology and oxidation stability properties of the NG/Cu NWs are provided in this study, and an efficient thermal conductivity of NG/Cu NWs was indicated using the laser flash method. In this way, the applications of the thermal interface materials (TIMs) and air-stable flexible electronic devices can be largely improved and expanded.

## 2. Materials and Methods

### 2.1. Materials

All the following chemicals were used as received without further purification: Sodium hydroxide was purchased from Alfa Aesar (35,633). Copper nitrate (Alfa Aesar, Haverhill, MA, USA, 10,699) was used as the copper precursor, ethylenediamine (EDA; Sigma Aldrich, St. Louis, MO, USA, E1521) was used as the structure-directing agent, and hydrazine (35 wt%, Sigma Aldrich, St. Louis, MO, USA, 309,400) was used as the reducing agent. The SiO<sub>2</sub>/Si wafer was purchased from LG Siltron Inc. Gumi, South Korea. (Silicon wafer; P/<100>, Boron) and was used as the substrate when we grew the N-doped graphene. The silicone elastomer (PDMS; Dow corning®, Midland, MI, USA, Sylgard 184 base & curing agent) was used as the polymer matrix when we fabricated TIMs.

### 2.2. Preparation of Cu NWs

The Cu NWs with diameters of 160–200 nm and length of ~25 μm were produced through an aqueous route according to a redox reaction [10,11]. In this study, 200 mL of sodium hydroxide solution (5 M), 10 mL of copper nitrate solution (0.1 M), and 1 mL EDA were added to a glass reactor, followed by thorough mixing of all reagents for 3 min. The reactor was placed in a water bath (60 °C), and then 500 μL of hydrazine was added into the reactor. After 1 h, the synthesis of Cu NWs was completed, and the Cu NWs were separated from the reaction solution by using a vacuum filtration system, in which a polyethersulfone (PES) membrane filter paper (pore size: 0.45 μm) was used. The Cu

NWs/PES membrane filter paper was dried at 80 °C in air. Here, the EDA with an amine group induces anisotropic growth of Cu, and can produce Cu wires. Thus, the Cu NWs with an amine group could be easily obtained from PES membrane filter paper.

### 2.3. Synthesis of the NG/Cu NWs

We used a T-CVD for fabricating NG/Cu NWs. Figure 1 shows the synthesis process of the NG/Cu NWs. Figure 1a shows the growth temperature of double zone, and the growth mechanism of the N-doped graphene in the quartz of the T-CVD. As shown Figure 1b, the as-grown Cu NWs were placed in the T-CVD quartz tube, which was heated up to 350 °C, to remove impurities, for 15 min. Here, we employed the DZGP in which the reactants heated at 900 °C in the first zone, flowed into the second zone and were maintained at 600 °C for the growth of N-doped graphene at a low temperature. In addition, the various partial pressures of CH<sub>4</sub> to maintain the morphology of Cu NWs with amine group were systematically examined. Next, we introduced the reaction gas mixture composed of Ar, H<sub>2</sub>, and CH<sub>4</sub> (4:1:1 and 10:2.5:1) into the quartz tube for 10 min. Here, the N-doped graphene was synthesized using the different carbon source (CH<sub>4</sub>) conditions (CH<sub>4</sub> flow; 20 and 50 sccm). After the cooling step, we could easily obtain the NG/Cu NWs.

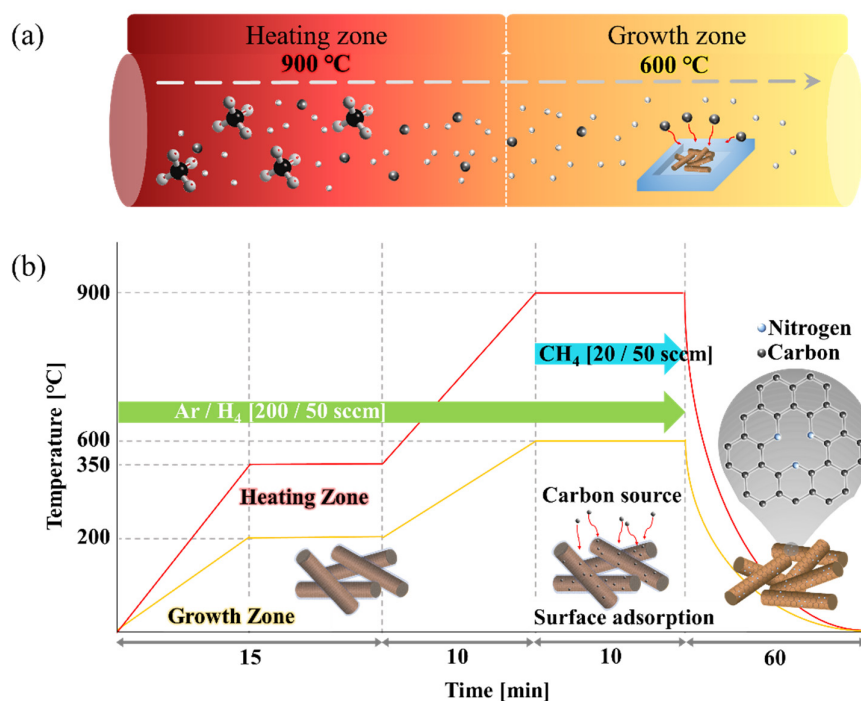


**Figure 1.** Schematic illustrations for processes in present work: (a) double zone growth method and (b) detailed method of graphene growth.

In addition, the heat-transfer materials were fabricated using as-grown Cu NWs, NG/Cu NWs synthesized with 20 sccm CH<sub>4</sub> (NG/Cu NWs;M20), and NG/Cu NWs synthesized with 50 sccm CH<sub>4</sub> (NG/Cu NWs;M50) for thermal conductivity measurements. The three prepared materials, epoxy matrix, and PDMS curing agent were mixed using a paste mixer for 10 min, and the pastes were then placed in oven at 120–180 °C for 30 min. Finally, we obtained three heat-transfer materials.

### 2.4. Characterization

The sheet resistances of as-grown Cu NWs, NG/Cu NWs;M20, and NG/Cu NWs;M50 were measured using a 4-point probe system (DASOL ENG, Chungcheongbuk-do, South Korea, FPP-HS 8). Raman spectra of NG/Cu NWs;M20 and NG/Cu NWs;M50 were obtained using a 532 nm excitation laser with spot diameter of 50 μm (JASCO, Tokyo, Japan, NRS-3300). An elemental composition

analysis was conducted using X-ray photoelectron spectroscopy (XPS, Thermal Fisher Scientific, Waltham, MA, USA, ESCALAB 250 XPS system, a monochromatic X-ray source, image resolution  $<3 \mu\text{m}$ ). Morphological properties of the three materials were investigated using a field emission scanning electron microscope (FE-SEM, Hitachi, Tokyo, Japan, S-4300), and the thermal conductivities were measured using a laser flash method (NETZSCH, Selb, Germany, LFA467, Temperature range from  $-100^\circ\text{C}$  to  $1250^\circ\text{C}$ , Xenon flash lamp; pulse energy: Up to 10 J/pulse, pulse width: 10 to 1500  $\mu\text{s}$ ).

### 3. Results and Discussion

In this work, an aqueous procedure was proposed to synthesize large-scale Cu NWs. We obtained approximately 53.3 mg of Cu NWs from 64.04 mg of Cu solution at one time. This result shows approximately 83.2% yield of Cu NWs. FE-SEM was used to observe the morphology of as-grown Cu NWs, as shown in Figure 2. The average diameter of the Cu NWs immediately after growth was about 400 nm and the average length was  $\sim 25 \mu\text{m}$ . Regrettably, the Cu NWs with high aspect ratio are easily oxidized in air [28–30], and the physical properties of Cu NWs are weakened by oxidation [20]. Therefore, we synthesized NG/Cu NWs via DZGP to inhibit oxidation. The average diameter of Cu NWs after graphene growth was reduced by the growth heat and the Cu NWs immediately after growth were about 200 nm. To evaluate the morphologies of NG/Cu NWs;M20 and NG/Cu NWs;M50 after DZGP, they were investigated using the FE-SEM. As shown in Figure 2c–f, Cu NWs were physically intact following the DZGP at low temperature. We observed the growth of a graphene shell on Cu NWs.

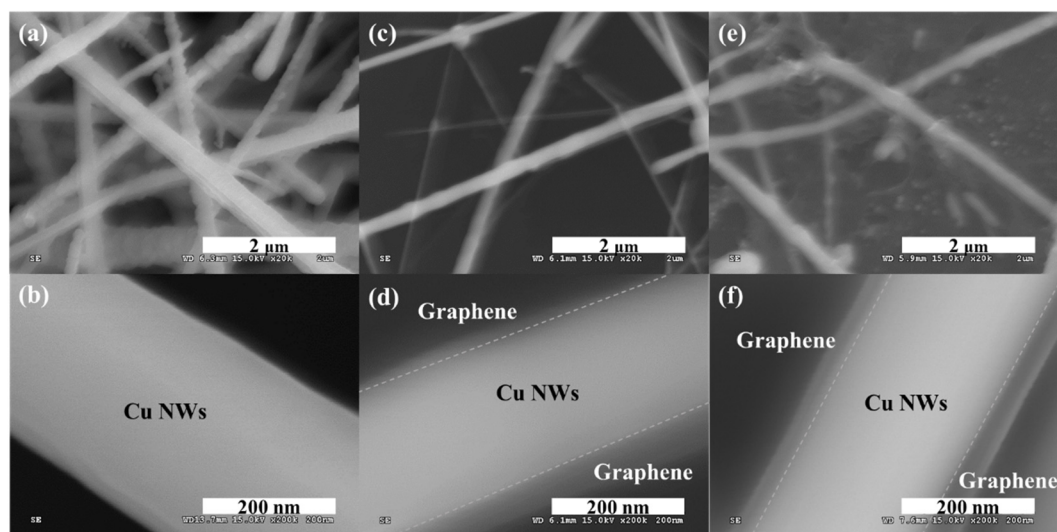


**Figure 2.** SEM images of (a,b): As-grown Cu NWs, (c,d): NG/Cu NWs;M20, and (e,f): NG/Cu NWs;M50.

The presence of graphene, the layer number, and degree of the defect level according to  $\text{CH}_4$  gas flow were investigated through Raman spectroscopy. Figure 3 displays the Raman spectra of the NG/Cu NWs;M20 and NG/Cu NWs;M50 measured at an excitation wavelength of 532 nm. We confirmed the presence of the characteristic Raman spectral peaks of graphene at  $1350$ ,  $1600$ , and  $2700 \text{ cm}^{-1}$  on the NG/Cu NWs;M20 and NG/Cu NWs;M50 samples. The Raman intensities showed the defect-band (D-band) of  $\text{sp}^3$  carbon bond and the graphite-bond (G-band) of the  $\text{sp}^2$  carbon bond. In general, the D-band is caused by the breathing mode of the  $\text{A}_{1g}$ -symmetry, and involving phonons near the K-zone boundary. However, the G-band is caused by the zone center phonons of the  $\text{E}_{2g}$ -symmetry [38]. There are many factors, such as doping, layer numbers, defects, strains, and substrate, which can affect the position of the D band. Moreover, our observations are similar to those of N-doped carbon nanotubes (CNTs), in which the degree of N doping causes an upshift of the D band and a downshift of the G band [33,34]. The high intensity of the D peak indicates the doping of the graphitic sheets [33,34],

as the D band only occurs in the  $sp^2$  C with defects [39], and N doping introduces large amounts of topological defects [35–37]. To gain a better insight into the G/Cu NWs, the broad Raman spectrum in the range  $1100$ – $2000$   $cm^{-1}$  was deconvoluted. In addition, four peaks, that is, D1, D2, D3, and D' were observed. The edge shows a special kind of disorder, and the nature of the edges could be probed with respect to the intensity of the D peak. The D peak arises from the momentum conservation law owing to the formation of edge states (zigzag and armchair). The many studies reported that the intensity of the D peak is very sensitive to the nature of edge states in graphene. The additional peaks D1, D2, and D3 may be associated with functional group defects. The D1 peaks of NG/Cu NWs;M20 and NG/Cu NWs;M50 at  $1197$  and  $1182$   $cm^{-1}$  were assigned to the  $sp^2$ – $sp^3$  bonded carbon atoms at the graphene edges [40–44]. The D2 peaks of NG/Cu NWs;M20 and NG/Cu NWs;M50 at  $1245$  and  $1248$   $cm^{-1}$  were assigned to COOH or ring-type C–OH edge functional groups [40–42], while the Raman D3 peaks at  $1514$  and  $1496$   $cm^{-1}$  were attributed to C=O/C–O functional groups [42,43]. The D' peak is attributed to the vacancies and/or pentagonal and octagonal defects, usually referred to as zigzag 5–7 defects, and represents the crystalline defects in graphene [33,42–44]. The D' peaks of NG/Cu NWs;M20 and NG/Cu NWs;M50 were centered at  $1607$  and  $1666$   $cm^{-1}$ . In addition, the 2D peak appeared when a non-elastic scattering phonon occurred after the second experiment, and the position of the 2D peak was dependent on the number of graphene layers [41,45]. Generally,  $I_{2D}/I_G$  ratio  $>2$  indicates the growth of monolayer graphene, while a value  $<2$  indicates the growth of bilayer graphene. As observed from Figure 3, the ratios of the  $I_{2D}/I_G$  peak intensities were  $0.11$  and  $0.09$  for the NG/Cu NWs;M20 and NG/Cu NWs;M50 samples, respectively. Therefore, based on the Raman characterization, the obtained results showed that the NG/Cu NWs;M20 and NG/Cu NWs;M50 samples resulted in N-doped graphene with multilayers on Cu NWs.

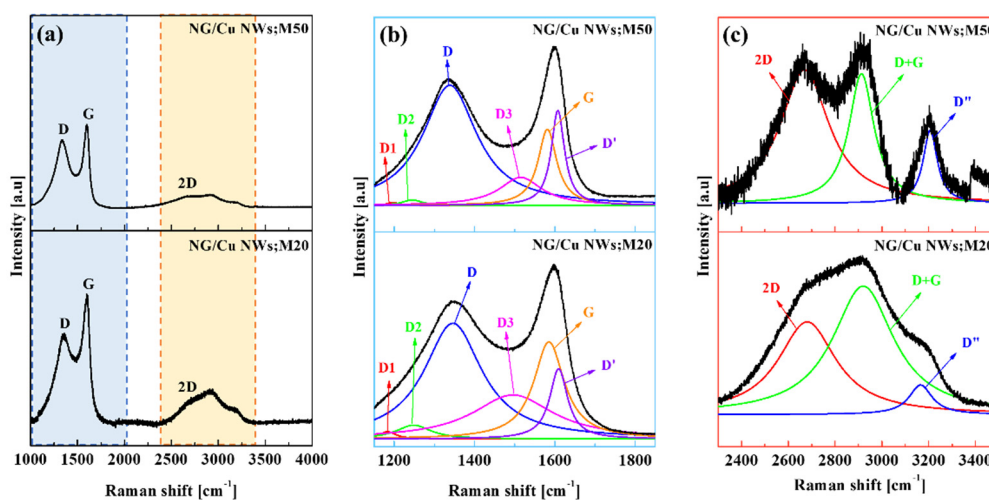


**Figure 3.** Raman spectra ranging from (a)  $1000$ – $4000$   $cm^{-1}$ , (b)  $1100$ – $1900$   $cm^{-1}$ , and (c)  $2300$ – $3500$   $cm^{-1}$ .

The XPS spectra showed the doping of the graphene. Figure 4 displays the high-resolution C 1s, N 1s, O 1s, and Cu  $2p_{3/2}$  spectra of Cu NWs, NG/Cu NWs;M20, and NG/Cu NWs;M50 samples. For as-grown Cu NWs, the C 1s spectra were observed because of the presence of EDA. As shown in Figure 5a, C  $sp^2$  peaks of all samples were centered at  $284.30$ ,  $284.53$ , and  $284.53$  eV, respectively. The main peak corresponds to the graphite-like C  $sp^2$ , indicating that most of the C atoms in the N-doped graphene were arranged in a conjugated honeycomb lattice. The C  $sp^2$  peak of as-grown Cu NWs was weaker than the C  $sp^3$  peak, whereas C  $sp^2$  peaks of NG/Cu NWs;M20 and NG/Cu NWs;M50 were much stronger than their C  $sp^3$  peaks. This indicates that most of the carbon atoms in NG/Cu NWs were arranged in a two-dimensional graphite-like honeycomb lattice [28,29]. The C  $sp^3$  peaks of all samples were located at  $284.83$ ,  $285.39$ , and  $285.39$  eV, respectively. The C  $sp^3$  peak of as-grown Cu NWs was stronger than the  $sp^2$  peak, suggesting that the EDA randomly bonded with

each other. The C  $sp^3$  peaks of NG/Cu NWs;M20 had a relatively smaller intensity than those of the NG/Cu NWs;M50. This was attributed to either crystalline or functional-group defects in G/Cu NWs, and corresponds to the N- $sp^3$  C bonds. In C 1s spectra of as-grown Cu NWs, the very small peaks at 286.23 and 288.95 eV were attributed to C–O and O–C=O, respectively. For C 1s spectra of NG/Cu NWs;M20 and NG/Cu NWs;M50, the broad peaks were attributed to C–O/C=N, which were located at 285.44 and 285.46 eV, respectively. Other peaks at 288.92 and 289.18 eV were attributed to the C–N functional group. The results indicated that the carbon atoms at the edge are reconstructed during the removal of impurities [46]. In addition, the carbon atoms were bonded with amine groups to maintain the stability of the carbon atoms at the graphene edges. As shown in Figure 5b, we confirmed four peaks in the as-grown Cu NWs, namely, pyridinic N, pyrrolic N, amino N, and oxygenated N, which are located at 398.07, 399.74, 400.70, and 404.14 eV, respectively. After DZGP, the N 1s spectra of NG/Cu NWs;M20 and NG/Cu NWs;M50 also showed four peaks: Pyridinic N, amino N, graphitic N, and oxygenated N. The pyridinic N peaks of NG/Cu NWs;M20 and NG/Cu NWs;M50 were centered at 398.65 and 398.03 eV, respectively.

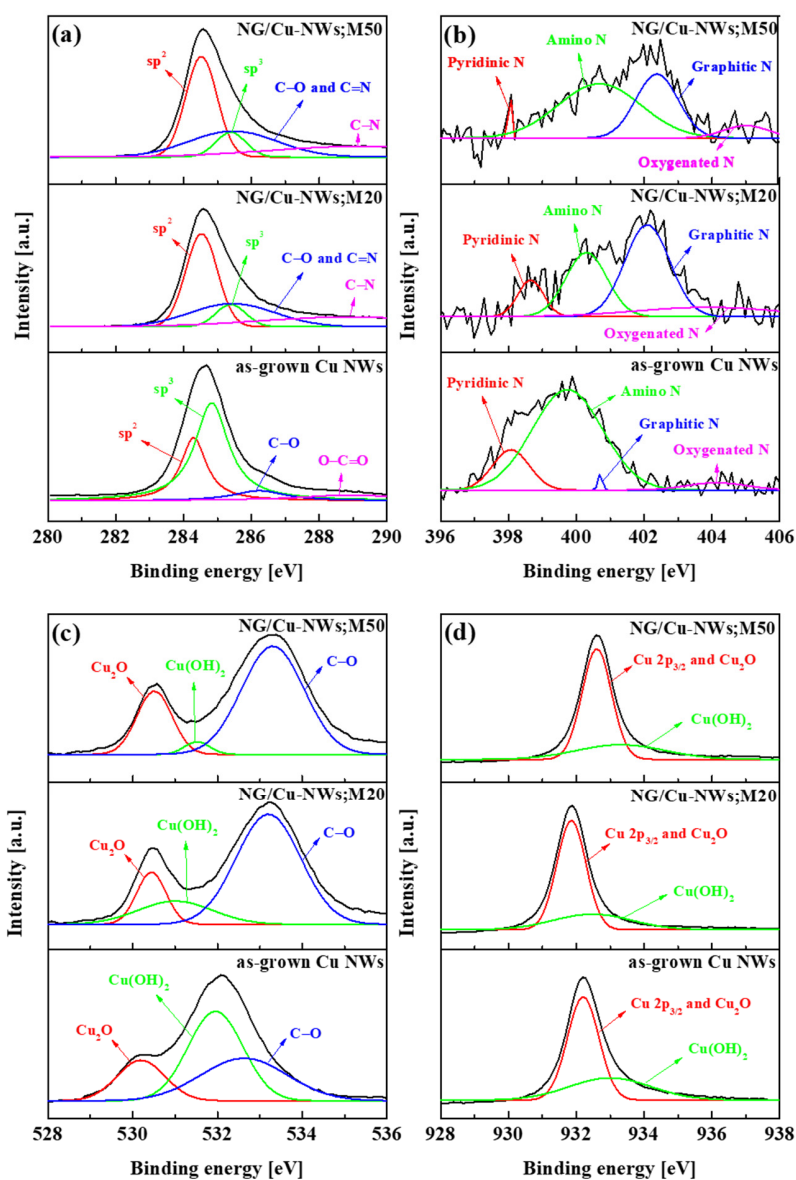


**Figure 4.** XPS spectra of as-grown Cu NWs, NG/Cu NWs;M20, and NG/Cu NWs;M50: high-resolution (a) C 1s, (b) N 1s, (c) O 1s, and (d) Cu  $2p_{3/2}$ .

The amino-N peaks were notably changed after DZGP. The amino-N peaks of NG/Cu NWs;M20 and NG/Cu NWs;M50 were located at 400.30 and 400.69 eV, respectively. The pyrrolic-N peak disappeared, while the graphitic-N peaks were newly generated. Here, the peaks refer to the N atoms located in a  $\pi$  conjugated system and contribute to the  $\pi$  system with one or two p-electrons, respectively [47,48]. The peak of graphitic N, which refers to the N atoms replacing the C atoms inside of the graphene layers [48], was much higher; thus, the N atoms are substitutionally doped into the graphene lattice and existed mainly in the form of graphitic N. The graphitic-N peaks in NG/Cu NWs;M20 and NG/Cu NWs;M50 were centered at 402.09 and 402.38 eV, respectively. As the amine groups on Cu NWs bonded with the carbon atoms, the amino N and pyrrolic N changed to graphitic N [49,50]. As shown in Figure 4c, the as-grown Cu NWs displayed three peaks, namely,  $\text{Cu}_2\text{O}$ ,  $\text{Cu}(\text{OH})_2$ , and C–O, which were located at 530.19, 531.95, and 532.63 eV, respectively. The  $\text{Cu}_2\text{O}$  peaks in NG/Cu NWs;M20 and NG/Cu NWs;M50 were centered at 530.44 and 530.51 eV, respectively. After the DZGP, the  $\text{Cu}(\text{OH})_2$  peaks were significantly changed, indicating that the Cu NWs were reduced because of the DZGP. In addition, the O 1s peak results from the oxygen or water absorbed on the surface of the N-doped graphene [47,51,52]. As shown in Figure 4d, the Cu  $2p_{3/2}$  spectrum of all samples showed a similar tendency; however, we observed that the peaks were shifted after the DZGP. These results show that we successfully grew the NG/Cu NWs due to the amine groups onto as-grown Cu NWs. Furthermore, the NG/Cu NWs;M50 sample showed a larger amount of N doping than the NG/Cu NWs;M20 sample.

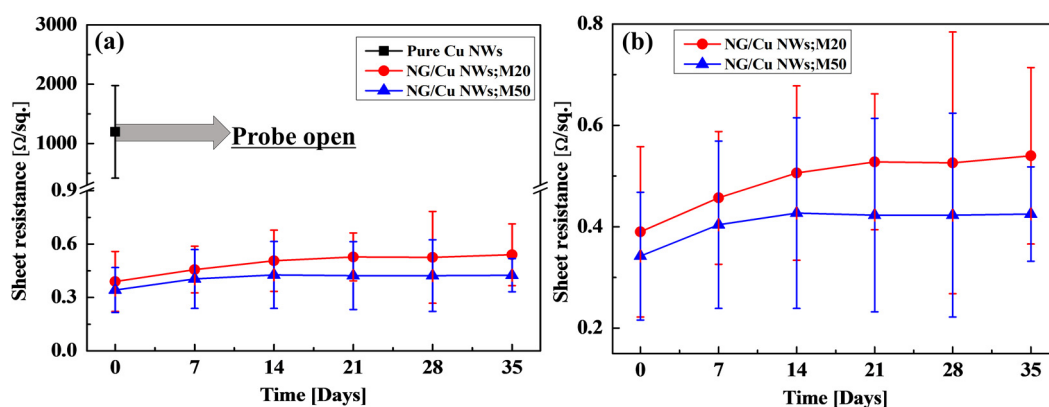


**Figure 5.** (a) Sheet resistance of the pure Cu NWs, NG/Cu NWs;M20, and NG/Cu NWs;M50 and (b) the enlarged sheet resistance of NG/Cu NWs;M20 and NG/Cu NWs;M50.

Additionally, the NG/Cu NWs;M20 and NG/Cu NWs;M50 samples were exposed to atmospheric conditions for several days to test their oxidation stability. The EDA with amine group on as-grown Cu NWs was removed using de-ionized (DI) water for observing the oxidation stability of pure Cu NWs. Figure 5a shows the sheet resistances of all samples. The pure Cu NWs were naturally oxidized immediately after the EDA was removed. However, the sheet resistances of NG/CuNWs;M20 and NG/Cu NWs;M50 were retained owing to the N-doped graphene-coated layer. Koo et al. [53] reported on the relationship between the EDA and oxidation of Cu NWs and suggested that the EDA, which is a growth source of N-doped graphene, could be suppressing the oxidation of Cu NWs. Figure 5b results show that the NG/Cu NWs;M50 sample with higher doping than the NG/Cu NWs;M20 sample shows characteristics of low sheet resistance and high oxidation prevention.

The as-grown Cu NWs, NG/Cu NWs;M20, and NG/Cu NWs;M50 were fabricated as the fillers in TIMs at 23 wt% for measuring thermal conductivity through the laser flash method. Table 1 shows the clear values of thermal conductivity and the TIMs sample name about sample number. Figure 6 displays the thermal conductivity of the TIMs. The measured thermal conductivity of the polymer matrix was 0.22 W/m·K. The thermal conductivities of NG/Cu NWs with M20 and M50 were 0.39 and 0.51 W/m·K,

respectively, showing an improvement by 75% and 130%, respectively. Moreover, the NG/Cu NWs;M50 sample showed good thermal conductivity than that of the previously studied TIMs.

**Table 1.** The thermal conductivity and the TIMs.

Sample No.	TIMs Sample Name	Thermal Conductivity [W/m·K]	Reference
1	MWCNT	0.23	[3]
2	Ag NWs	0.42	[4]
3	Graphene nanoplates	0.465	[1]
4	SWCNT	0.5	[2]
5	Cu NWs	0.41	[54]
6	NG/Cu NWs;M20	0.387	In this study
7	NG/Cu NWs;M50	0.505	In this study
8	Polymer matrix (Epoxy)	0.221	In this study

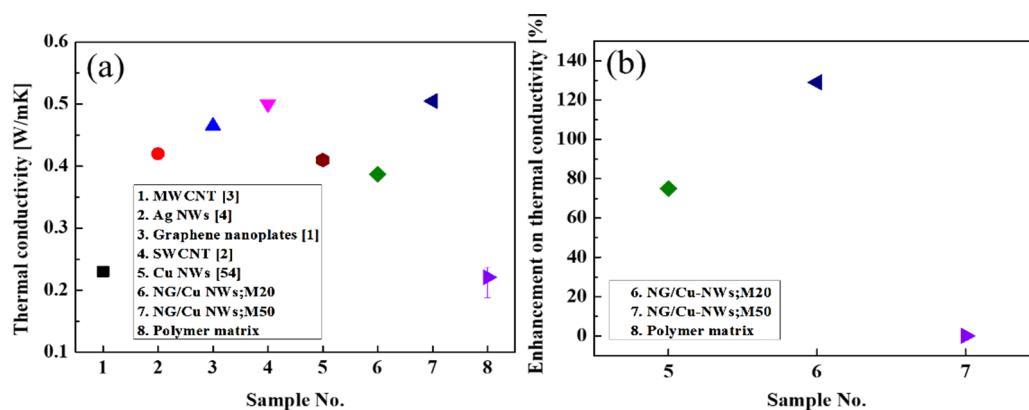


**Figure 6.** (a) Thermal conductivity of the two TIMs used in this study and the TIMs of other studies. (b) Enhancement of thermal conductivity of the two TIMs used in the current study from the polymer matrix.

#### 4. Conclusions

In this study, we synthesized Cu NWs with diameters of 160–200 nm and lengths of ~25  $\mu\text{m}$ . To avoid the rapid oxidation and changing of the morphology of the Cu NWs, we succeeded in synthesizing NG/Cu NWs according to two  $\text{CH}_4$  gas flow methods by using DZGP at low growth temperature of approximately 600  $^\circ\text{C}$ . The morphology of NG/Cu NWs was confirmed to be well preserved. N doping for graphene was successfully conducted through amine groups on as-grown Cu NWs and confirmed by Raman spectra and XPS measurement. The TIMs with three NG/Cu NWs;M20 and NG/Cu NWs;M50 as fillers were prepared using a paste mixer, and their thermal conductivity values were measured using a laser flash method. The thermal conductivity values of the heat-transfer materials (TIMs) with NG/Cu NWs;M20 and NG/Cu NWs;M50 are measured to be 0.39 and 0.51 W/m·K, respectively, indicating an improvement of 75% and 130%, respectively, compared with the polymer matrix (0.22 W/m·K). Especially, the NG/Cu NWs;M50 sample showed good thermal conductivity than that of the previously studied TIMs [1–4,54]. The results showed that the synthesis technology of the N-doped graphene on Cu NWs could promote future research and applications in the TIMs and air-stable flexible electronic devices.

**Author Contributions:** Conceptualization and writing—original draft, M.P.; validation and investigation, S.-K.A. and S.H.; data curation and formal analysis, S.P. and S.K.; supervision and writing—review and editing, M.J.

**Funding:** “This research was supported by a grant to Bio-Mimetic Robot Research Center Funded by Defense Acquisition Program Administration, and by Agency for Defense Development (UD1300701D)” and “This research was supported by Basic Science Research Program through the National Research Foundation of Korea (NRF) funded by the Ministry of Education (NRF-2016R1D1A1B01011724)”.

**Conflicts of Interest:** The authors declare no conflicts of interest.

## References

1. Wang, S.; Cheng, Y.; Wang, R.; Sun, J.; Gao, L. Highly thermal conductive copper nanowire composites with ultralow loading: Toward applications as thermal interface materials. *ACS Appl. Mater. Interfaces* **2014**, *6*, 6481–6486. [[CrossRef](#)] [[PubMed](#)]
2. Hansson, J.; Nilsson, T.M.J.; Ye, L.; Liu, J. Novel nanostructured thermal interface materials: A review. *Int. Mater. Rev.* **2017**, *63*, 22–45. [[CrossRef](#)]
3. Balachander, N.; Seshadri, I.; Mehta, R.J.; Schadler, L.S.; Borca-Tasciuc, T.; Koblinski, P.; Ramanath, G. Nanowire-filled polymer composites with ultrahigh thermal conductivity. *Appl. Phys. Lett.* **2013**, *102*, 093117. [[CrossRef](#)]
4. Xing, Y.; Cao, W.; Li, W.; Chen, H.; Miao, W.; Wei, H.; Hu, D.; Chen, M.; Li, Q. Carbon nanotube/Cu nanowires/epoxy composite mats with improved thermal and electrical conductivity. *J. Nanosci. Nanotechnol.* **2015**, *15*, 3265–3270. [[CrossRef](#)] [[PubMed](#)]
5. Ahn, K.; Kim, K.; Kim, J. Thermal conductivity and electric properties of epoxy composites filled with TiO<sub>2</sub>-coated copper nanowire. *Polymer* **2015**, *76*, 313–320. [[CrossRef](#)]
6. Chen, W.; Wang, Z.; Zhi, C.; Zhang, W. High thermal conductivity and temperature probing of copper nanowire/upconversion nanoparticles/epoxy composite. *Compos. Sci. Technol.* **2016**, *130*, 63–69. [[CrossRef](#)]
7. Rai, A.; Moore, A.L. Enhanced thermal conduction and influence of interfacial resistance within flexible high aspect ratio copper nanowire/polymer composites. *Compos. Sci. Technol.* **2017**, *144*, 70–78. [[CrossRef](#)]
8. Xu, X.; Pereira, L.F.C.; Wang, Y.; Wu, J.; Zhang, K.; Zhao, X.; Bae, S.; Bui, C.T.; Xie, R.; Thong, J.T.L.; et al. Length-dependent thermal conductivity in suspended single-layer graphene. *Nat. Commun.* **2014**, *5*, 3689. [[CrossRef](#)]
9. Zhao, Y.; Zhang, Y.; Li, Y.; Yan, Z. Soft synthesis of single-crystal copper nanowires of various scales. *New J. Chem.* **2012**, *36*, 130–138. [[CrossRef](#)]
10. Chang, Y.; Lye, M.L.; Zeng, H.C. Large-scale synthesis of high-quality ultralong copper nanowires. *Langmuir* **2005**, *21*, 3746–3748. [[CrossRef](#)]
11. Rathmell, A.R.; Bergin, S.M.; Hua, Y.L.; Li, Z.Y.; Wiley, B.J. The growth mechanism of copper nanowires and their properties in flexible, transparent conducting films. *Adv. Mater.* **2010**, *22*, 3558–3563. [[CrossRef](#)] [[PubMed](#)]
12. Zhang, D.; Wang, R.; Wen, M.; Weng, D.; Cui, X.; Sun, J.; Li, H.; Lu, Y. Synthesis of ultralong copper nanowires for high-performance transparent electrodes. *J. Am. Chem. Soc.* **2012**, *134*, 14283–14286. [[CrossRef](#)] [[PubMed](#)]
13. Li, S.; Chen, Y.; Huang, L.; Pan, D. Large-scale synthesis of well-dispersed copper nanowires in an electric pressure cooker and their application in transparent and conductive networks. *Inorg. Chem.* **2014**, *53*, 4440–4444. [[CrossRef](#)] [[PubMed](#)]
14. Tang, X.F.; Yang, Z.G.; Wang, W.J. A simple way of preparing high-concentration and high-purity nano copper colloid for conductive ink in inkjet printing technology. *Colloids Surf. A Physicochem. Eng. Asp.* **2010**, *360*, 99–104. [[CrossRef](#)]
15. Jeong, S.; Lee, S.H.; Jo, Y.; Lee, S.S.; Seo, Y.H.; Ahn, B.W.; Kim, G.; Jang, G.E.; Park, J.U.; Ryu, B.H.; et al. Air-stable, surface-oxide free Cu nanoparticles for highly conductive Cu ink and their application to printed graphene transistors. *J. Mater. Chem. C* **2013**, *1*, 2704–2710. [[CrossRef](#)]
16. Wang, G.; Ru, G.; Wan, G.; Yang, P.; Gao, Z.; Lin, S.; Fu, C.; Qin, Y. Size-selective catalytic growth of nearly 100% pure carbon nanocoils with copper nanoparticles produced by atomic layer deposition. *ACS Nano* **2014**, *8*, 5330–5338. [[CrossRef](#)] [[PubMed](#)]
17. Xu, S.; Man, B.; Jiang, S.; Wang, J.; Wei, J.; Xu, S.; Liu, H.; Gao, S.; Liu, H.; Li, Z.; et al. Graphene/Cu nanoparticle hybrids fabricated by chemical vapor deposition as surface-enhanced Raman scattering substrate for label-free detection of adenosine. *ACS Appl. Mater. Interfaces* **2015**, *7*, 10977–10987. [[CrossRef](#)]
18. Pashayi, K.; Fard, H.R.; Lai, F.; Iruvanti, S.; Plawsky, J.; Borca-Tasciuc, T. High thermal conductivity epoxy-silver composites based on self-constructed nanostructured metallic networks. *J. Appl. Phys.* **2012**, *111*, 104310. [[CrossRef](#)]
19. Castellino, M.; Chiolerio, A.; Shahzad, M.I.; Jagdale, P.V.; Tagliaferro, A. Electrical conductivity phenomena in an epoxy resin-carbon-based materials composite. *Compos. A Appl. Sci. Manuf.* **2014**, *61*, 108–114. [[CrossRef](#)]

20. Sachse, C.; Weiß, N.; Gaponik, N.; Müller-Meskamp, L.; Eychmüller, A.; Leo, K. ITO-Free, Small-Molecule Organic Solar Cells on Spray-Coated Copper-Nanowire-Based Transparent Electrodes. *Adv. Energy Mater.* **2014**, *4*, 1300737. [[CrossRef](#)]
21. Xu, W.H.; Wang, L.; Guo, Z.; Chen, X.; Liu, J.; Huang, X.J. Copper nanowires as nanoscale interconnects: Their stability, electrical transport, and mechanical properties. *ACS Nano* **2014**, *9*, 241–250. [[CrossRef](#)] [[PubMed](#)]
22. Rathmell, A.R.; Nguyen, M.; Chi, M.; Wiley, B.J. Synthesis of oxidation-resistant cupronickel nanowires for transparent conducting nanowire networks. *Nano Lett.* **2012**, *12*, 3193–3199. [[CrossRef](#)] [[PubMed](#)]
23. Kholmanov, I.N.; Domingues, S.H.; Chou, H.; Wang, X.; Tan, C.; Kim, J.Y.; Li, H.; Piner, R.; Zarbin, A.J.G.; Ruoff, R.S. Reduced graphene oxide/copper nanowire hybrid films as high-performance transparent electrodes. *ACS Nano* **2013**, *7*, 1811–1816. [[CrossRef](#)] [[PubMed](#)]
24. Mayousse, C.; Celle, C.; Carella, A.; Simonato, J.P. Synthesis and purification of long copper nanowires. Application to high performance flexible transparent electrodes with and without PEDOT: PSS. *Nano Res.* **2014**, *7*, 315. [[CrossRef](#)]
25. Im, H.G.; Jung, S.H.; Jin, J.; Lee, D.; Lee, J.; Lee, D.; Lee, J.Y.; Kim, I.D.; Bae, B.S. Flexible Transparent Conducting Hybrid Film Using a Surface-Embedded Copper Nanowire Network: A Highly Oxidation-Resistant Copper Nanowire Electrode for Flexible Optoelectronics. *ACS Nano* **2014**, *8*, 10973–10979. [[CrossRef](#)] [[PubMed](#)]
26. Song, J.; Li, J.; Xu, J.; Zeng, H. Super stable Transparent Conductive Cu@Cu<sub>4</sub>Ni Nanowire Elastomer Composites against Oxidation, Bending, Stretching, and Twisting for Flexible and Stretchable Optoelectronics. *Nano Lett.* **2014**, *14*, 6298–6305. [[CrossRef](#)] [[PubMed](#)]
27. Ye, S.; Stewart, I.E.; Chen, Z.; Li, B.; Rathmell, A.R.; Wiley, B.J. How copper nanowires grow and how to control their properties. *Acc. Chem. Res.* **2016**, *49*, 442–451. [[CrossRef](#)] [[PubMed](#)]
28. Ahn, Y.; Jeong, Y.; Lee, D.; Lee, Y. Copper nanowire–graphene core–shell nanostructure for highly stable transparent conducting electrodes. *ACS Nano* **2015**, *9*, 3125–3133. [[CrossRef](#)]
29. Dou, L.; Cui, F.; Yu, Y.; Khanarian, G.; Eaton, S.W.; Yang, Q.; Resasco, J.; Schildknecht, C.; Schierle-Arndt, K.; Yang, P. Solution-processed copper/reduced-graphene-oxide core/shell nanowire transparent conductors. *ACS Nano* **2016**, *10*, 2600–2606. [[CrossRef](#)]
30. Mehta, R.; Chugh, S.; Chen, Z. Enhanced electrical and thermal conduction in graphene-encapsulated copper nanowires. *Nano Lett.* **2015**, *15*, 2024–2030. [[CrossRef](#)]
31. Uchoa, B.; Neto, A.H.C. Superconducting states of pure and doped graphene. *Phys. Rev. Lett.* **2007**, *98*, 146801. [[CrossRef](#)] [[PubMed](#)]
32. Peres, N.M.R.; Guinea, F.; Neto, A.H.C. Coulomb interactions and ferromagnetism in pure and doped graphene. *Phys. Rev. B* **2005**, *72*, 174406. [[CrossRef](#)]
33. Keskar, G.; Rao, R.; Luo, J.; Hudson, J.; Chen, J.; Rao, A.M. Growth, nitrogen doping and characterization of isolated single-wall carbon nanotubes using liquid precursors. *Chem. Phys. Lett.* **2005**, *412*, 269–273. [[CrossRef](#)]
34. Yang, Q.H.; Hou, P.X.; Unno, M.; Yamauchi, S.; Saito, R.; Kyotani, T. Dual Raman features of double coaxial carbon nanotubes with N-doped and B-doped multiwalls. *Nano Lett.* **2005**, *5*, 2365–2469. [[CrossRef](#)] [[PubMed](#)]
35. Suenaga, K.; Yudasaka, M.; Colliex, C.; Iijima, S. Radially modulated nitrogen distribution in CN<sub>x</sub> nanotubular structures prepared by CVD using Ni phthalocyanine. *Chem. Phys. Lett.* **2000**, *316*, 365–372. [[CrossRef](#)]
36. Lee, Y.T.; Kim, N.S.; Bae, S.Y.; Park, J.; Yu, S.C.; Ryu, H.; Lee, H.J. Growth of Vertically Aligned Nitrogen-Doped Carbon Nanotubes: Control of the Nitrogen Content over the Temperature Range 900–1100 °C. *J. Phys. Chem. B* **2003**, *107*, 12958–12963. [[CrossRef](#)]
37. Wei, D.; Liu, Y.; Cao, L.; Fu, L.; Li, X.; Wang, Y.; Yu, G.; Zhu, D. A new method to synthesize complicated multibranch carbon nanotubes with controlled architecture and composition. *Nano Lett.* **2006**, *6*, 186–192. [[CrossRef](#)]
38. Erdem, E.; Mass, V.; Gembus, A.; Schulz, A.; Liebau-Kunzmann, V.; Fasel, C.; Riedel, R.; Eichel, R.A. Defect structure in lithium-doped polymer-derived SiCN ceramics characterized by Raman and electron paramagnetic resonance spectroscopy. *Phys. Chem. Chem. Phys.* **2009**, *11*, 5628–5633. [[CrossRef](#)]
39. Thomsen, C.; Reich, S. Double resonant Raman scattering in graphite. *Phys. Rev. Lett.* **2000**, *85*, 5214. [[CrossRef](#)]
40. Ferrari, A.C. Raman spectroscopy of graphene and graphite: Disorder, electron–phonon coupling, doping and nonadiabatic effects. *Solid State Commun.* **2007**, *143*, 47–57. [[CrossRef](#)]

41. Ferrari, A.C.; Meyer, J.C.; Scardaci, V.; Casiraghi, C.; Lazzeri, M.; Mauri, F.; Piscanec, S.; Jiang, D.; Novoselov, K.S.; Roth, S.; et al. Raman spectrum of graphene and graphene layers. *Phys. Rev. Lett.* **2006**, *97*, 187401. [[CrossRef](#)] [[PubMed](#)]
42. Sadezky, A.; Muckenhuber, H.; Grothe, H.; Niessner, R.; Pöschl, U. Raman microspectroscopy of soot and related carbonaceous materials: Spectral analysis and structural information. *Carbon* **2005**, *43*, 1731–1742. [[CrossRef](#)]
43. Bokobza, L.; Bruneel, J.L.; Couzi, M. Raman spectra of carbon-based materials (from graphite to carbon black) and of some silicone composites. *J. Carbon Res.* **2015**, *1*, 77–94. [[CrossRef](#)]
44. Eckmann, A.; Felten, A.; Mishchenko, A.; Britnell, L.; Krupke, R.; Novoselov, K.S.; Casiraghi, C. Probing the nature of defects in graphene by Raman spectroscopy. *Nano Lett.* **2012**, *12*, 3925–3930. [[CrossRef](#)]
45. Malard, L.M.; Pimenta, M.A.; Dresslhaus, G.; Dresslhaus, M.S. Raman spectroscopy in graphene. *Phys. Rep.* **2009**, *473*, 51–87. [[CrossRef](#)]
46. Rajender, G.; Giri, P.K. Formation mechanism of graphene quantum dots and their edge state conversion probed by photoluminescence and Raman spectroscopy. *J. Mater. Chem. C* **2016**, *4*, 10852–10865. [[CrossRef](#)]
47. Wang, X.; Liu, Y.; Zhu, D.; Zhang, L.; Ma, H.; Yao, N.; Zhang, B. Controllable Growth, Structure, and Low Field Emission of Well-Aligned CN<sub>x</sub> Nanotubes. *J. Phys. Chem. B* **2002**, *106*, 2186–2190. [[CrossRef](#)]
48. Casanovas, J.; Ricart, J.M.; Rubio, J.; Illas, F.; Jiménez-Mateos, J.M. Origin of the large N 1s binding energy in X-ray photoelectron spectra of calcined carbonaceous materials. *J. Am. Chem. Soc.* **1996**, *118*, 8071–8976. [[CrossRef](#)]
49. Wang, H.; Maiyalagan, T.; Wang, X. Review on recent progress in nitrogen-doped graphene: Synthesis, characterization, and its potential applications. *ACS Catal.* **2012**, *2*, 781–794. [[CrossRef](#)]
50. Jiang, Z.; Jiang, Z.J.; Tian, X.; Chen, W. Amine-functionalized holey graphene as a highly active metal-free catalyst for the oxygen reduction reaction. *J. Mater. Chem. A* **2014**, *2*, 441–450. [[CrossRef](#)]
51. Novoselov, K.S.; Geim, A.K.; Morozov, S.V.; Jiang, D.A.; Zhang, Y.; Dubonos, S.V.; Grigorieva, I.V.; Firsov, A.A. Electric field effect in atomically thin carbon films. *Science* **2004**, *306*, 666–669. [[CrossRef](#)] [[PubMed](#)]
52. Fu, L.; Liu, Z.; Liu, Y.; Han, B.; Hu, P.; Cao, L.; Zhu, D. Beaded cobalt oxide nanoparticles along carbon nanotubes: Towards more highly integrated electronic devices. *Adv. Mater.* **2005**, *17*, 217–221. [[CrossRef](#)]
53. Koo, J.; Kwon, S.; Kim, N.R.; Shin, K.; Lee, H.M. Ethylenediamine-Enhanced Oxidation Resistivity of a Copper Surface during Water-Based Copper Nanowire Synthesis. *J. Phys. Chem. C* **2016**, *120*, 3334–3340. [[CrossRef](#)]
54. Zhu, D.; Yu, W.; Du, H.; Chen, L.; Li, Y.; Xie, H. Thermal conductivity of composite materials containing copper nanowires. *J. Nanomater.* **2016**, *2016*, 8. [[CrossRef](#)]

